REPORT

CYTOSKELETON

Microtubules acquire resistance from mechanical breakage through intralumenal acetylation

Zhenjie Xu,[1,2]*† Laura Schaedel,[3] Didier Portran,[1] Andrea Aguilar,[1] Jérémie Gaillard,[3] M. Peter Marinkovich,[2,4] Manuel Théry,[3,5] Maxence V. Nachury[1]†

Eukaryotic cells rely on long-lived microtubules for intracellular transport and as compression-bearing elements. We considered that long-lived microtubules are acetylated inside their lumen and that microtubule acetylation may modify microtubule mechanics. Here, we found that tubulin acetylation is required for the mechanical stabilization of long-lived microtubules in cells. Depletion of the tubulin acetyltransferase TAT1 led to a significant increase in the frequency of microtubule breakage. Nocodazole-resistant microtubules lost upon removal of acetylation were largely restored by either pharmacological or physical removal of compressive forces. In in vitro reconstitution experiments, acetylation was sufficient to protect microtubules from mechanical breakage. Thus, acetylation increases mechanical resilience to ensure the persistence of long-lived microtubules.

How some cytoplasmic microtubules are stabilized and persist for several hours remains an open question (*1*). After stabilization, microtubules are posttranslationally detyrosinated and acetylated on lysine 40 of α-tubulin (αK40). Although detyrosination alters the binding site for microtubule-associated proteins (MAPs), severing enzymes, and motors to create specialized microtubule tracks (*2*), the molecular consequences of αK40 acetylation remain elusive. It is difficult to conceptualize how the modification of a residue inaccessible from outside the microtubule could alter MAP and motor binding (*2*, *3*). We recently proposed that acetylation modifies microtubule mechanics by weakening interprotofilament interactions (*4*).

TAT1 is responsible for nearly all acetylation on αK40 in every organism studied (*2*). Although TAT1 depletion from retinal pigment epithelial (RPE) cells did not measurably affect global microtubule polymerization or organization (fig. S1), tubulin detyrosination was significantly decreased at the bulk level (Fig. 1A and fig. S2, A and B) and reduced on microtubules of TAT1-depleted cells (Fig. 1B) and *Tat1*$^{-/-}$ mouse embryonic fibroblasts (MEFs) (fig. S2C). Given that acetylation and detyrosination sites are separated by the microtubule wall, it is unlikely that the two modifications are enzymatically coupled. Instead, long-lived microtubules, including detyrosinated microtubules, may be lost when acetylation is reduced. After treating cells with nocodazole, dynamic microtubules were depolymerized, and most remaining microtubules displayed the typical characteristics of long-lived microtubules with high levels of acetylation and detyrosination and long and curvy morphology (Fig. 1C and fig. S2D). Under the same conditions, very few microtubules remained in TAT1-depleted cells, and these were very short and dispersed throughout the cell (Fig. 1C). The number of microtubules that remained after nocodazole treatment was significantly decreased upon TAT1 depletion in RPE cells (Fig. 1D) or in *Tat1*$^{-/-}$ MEFs (fig. S2, E and F). The effect of TAT1 removal was even more striking when the length of nocodazole-resistant microtubules was examined (Fig. 1E). After 60 min of nocodazole treatment, most microtubules were normally longer than 4 μm but shorter than 2 μm in TAT1-depleted cells.

Because pharmacological reduction of tubulin detyrosination did not affect the length of nocodazole-resistant microtubules or the levels of acetylation (fig. S3), the effects of TAT1 depletion on nocodazole-resistant microtubules are unlikely to be caused by the observed reduction in detyrosination. Because overexpression of TAT1—but not a catalytically dead mutant—significantly elevated the mass of nocodazole-resistant microtubules (fig. S4) and because nocodazole-resistant microtubules are increased in MEFs that lack the tubulin deacetylase HDAC6 (*5*), it is αK40 acetylation rather than an acetyltransferase-independent activity of TAT1 (*6*–*8*) that is required for the maintenance of long-lived cytoplasmic microtubules in mammalian cells. Long-lived microtubules are not lost from TAT1-depleted cells because of an increased susceptibility to severing enzymes, because acetylation does not influence the activity of spastin in vitro (*9*) and did not affect the activity of spastin or katanin in vivo (fig. S5). Defective centrosomal microtubule anchoring in TAT1-depleted cells was ruled out by imaging microtubule regrowth after depolymerization (fig. S6).

Long-lived microtubules display frequent buckling because of compressive forces generated by microtubule-based motors and actomyosin contractility (*10*–*12*). Because microtubules are very stiff polymers that rupture when subjected to flexural stresses (*13*), this highly bent morphology suggests the existence of protective mechanisms for long-lived microtubules. The repair of lattice defects has emerged as an intrinsic property of microtubules that are subjected to mechanical stress (*14*, *15*), and acetylation protects microtubules from mechanical fatigue in vitro (*4*). A further suggestion that acetylation may confer mechanical protection to microtubules comes from the observation that removing TAT-1 from touch receptor neurons of nematodes results in profound microtubule lattice defects (*6*, *16*) that can be rescued by paralyzing the animals (*8*). Finally, although detyrosination is evenly distributed along microtubules (fig. S7A) (*17*), the pattern of acetylation is discontinuous with a preference for highly curved areas of nocodazole-resistant microtubules (Fig. 1, F and G, and fig. S7B), suggesting that TAT1 may preferentially acetylate segments experiencing stress. Alternatively, it is conceivable that only bends at regions that are acetylated were preserved after fixation (see the supplementary text). Localized acetylation is thus a prime candidate for the mechanical adaptation of microtubules to mechanical stresses.

We sought to test the hypothesis that long-lived microtubules disappear in the absence of TAT1 because of an increased rate of breakage under mechanical stress. In the past, imaging of microtubule breakage has been limited to very thin areas of the cell, such as lamellipodia, where single microtubules can be readily resolved (*11*, *18*, *19*). However, most of the microtubules in lamellipodia are dynamic and thus not acetylated (*20*). To specifically image the breakage of long-lived microtubules, we followed microtubules in real time in the presence of nocodazole using a triple green fluorescent protein (GFP) fusion with the microtubule-binding domain of ensconsin (EMTB), a MAP that does not affect microtubule dynamics when expressed at low levels (*21*). After 15 min in nocodazole, most remaining microtubules were highly bent, acetylated, and detyrosinated (fig. S7A), and microtubule number was similar in control and TAT1-depleted RPE-[EMTB-GFP^{3}] cells (fig. S8, A and B). Over the next 30 min of live cell imaging, microtubules rapidly disappeared in TAT1-depleted cells, whereas most microtubules persisted in control cells (fig. S8, A

[1]Department of Molecular and Cellular Physiology, Stanford University School of Medicine, Stanford, CA 94305-5345, USA. [2]Program in Epithelial Biology, Stanford University School of Medicine, Stanford, CA 94305-5168, USA. [3]CytoMorpho Laboratory, Laboratory of Cell and Plant Physiology (LPCV), UMR 5168, Biosciences and Biotechnology Institute of Grenoble, CEA/INRA/CNRS/Université Grenoble-Alpes, 17 rue des Martyrs, 38054 Grenoble, France. [4]Division of Dermatology, Palo Alto Veterans Affairs Medical Center, Palo Alto, CA 94305, USA. [5]CytoMorpho Laboratory, A2T, UMRS 1160, Institut Universitaire d'Hématologie, Hôpital Saint Louis, INSERM/AP-HP/Université Paris Diderot, 1 Avenue Claude Vellefaux, 75010 Paris, France.
*Present address: Department of Anatomy, University of California, San Francisco, CA 94143-0452, USA. †**Corresponding author.** **Email: nachury@gmail.com (M.V.N.); zhenjie.xu@gmail.com (Z.X.)**

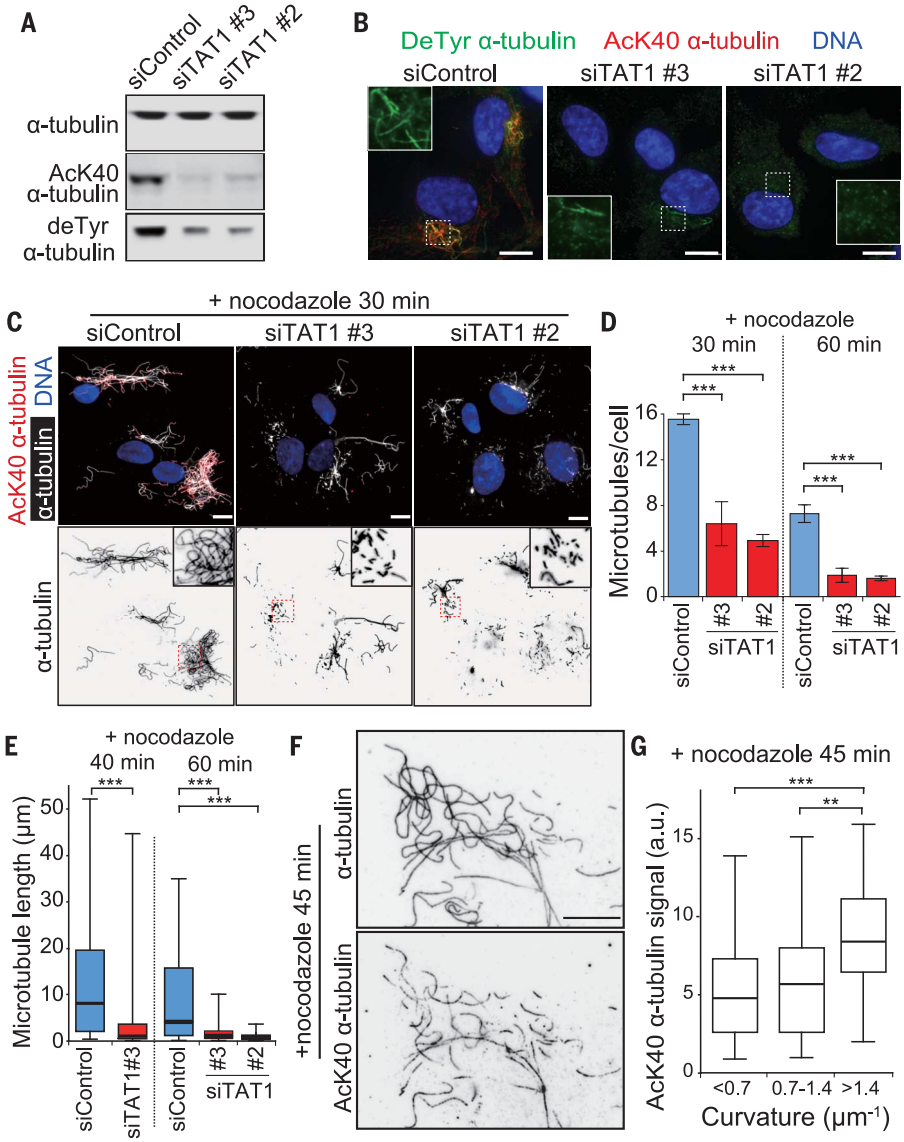

Fig. 1. Long-lived microtubules are lost in the absence of α-tubulin K40 acetylation. (**A**) α-Tubulin K40 acetylation and detyrosination levels were measured by immunoblotting lysates of RPE cells treated with two different small interfering RNAs (siRNAs) against TAT1 (siTAT1 #2 and siTAT1 #3) or control siRNAs (siControl). (**B**) Immunofluorescence (IF) images of siRNA-treated RPE cells stained for acetylated α-tubulin K40 (red), detyrosinated tubulin (green), and DNA (blue). Scale bar, 10 μm. Insets are 7 by 7 μm. (**C**) IF images of siRNA-treated RPE cells treated with 2 μM nocodazole and stained for α-tubulin (white), acetylated α-tubulin (red), and DNA (blue). (Bottom) The α-tubulin channel alone. (Insets) The highly curved microtubules present in control cells and the very short microtubules in TAT1-depleted cells. Scale bar, 10 μm (main panels). Insets are 10 by 10 μm. The number (**D**) and length (**E**) of microtubules remaining after nocodazole treatment were measured in siRNA-treated RPE cells. (**D**) *N* (30 min) = 153 (siCTRL), 157 (siTAT1 #3), and 155 (siTAT1 #2) cells, four independent experiments; *N* (60 min) = 236 (siCTRL), 302 (siTAT1 #3) and 206 (siTAT #2) cells, three independent experiments. Error bars indicate SD. Asterisks indicate *t* test significance values; $^{***}P < 10^{-4}$. (**E**) The box is bound by the 25th to 75th percentile, whiskers span 5th to 95th percentile, and the bar in the middle is the median. *N* (40 min) = 3058 (siControl), 4659 (siTAT1#3) microtubules from at least 500 cells, six independent experiments; *N* (60 min) = 880 (siControl), 1783 (siTAT1#3) and 1323 (siTAT1#2) microtubules from at least 180 cells, three independent experiments. Asterisks indicate Mann-Whitney *U* test significance values; $^{***}P < 10^{-4}$. (**F**) IF images of RPE cells treated with nocodazole for 45 min and stained for acetylated α-tubulin and α-tubulin. Scale bar, 10 μm. (**G**) The level of α-tubulin K40 acetylation and the curvature were measured along microtubules in IF images of cells treated with nocodazole for 45 min. The whiskers indicate 1.5 times the range. *N* = 1904 data points from 23 microtubules. Asterisks indicate Mann-Whitney *U* test significance values; $^{**}P < 10^{-3}$, $^{***}P < 10^{-4}$.

and C) and the mean microtubule length was significantly decreased in TAT1-depleted cells after 50 min in nocodazole (fig. S8D). Consistent with prior observations of microtubule breakage in fibroblasts (*18*, *19*), typical rupture events (Fig. 2, A to C; fig. S9, A and B; and movies S5 to S9) were preceded by local microtubule buckling, with the breakage site coinciding with the region of highest curvature. Tracking individual microtubules demonstrated that the frequency of microtubule breakage events preceded by buckling was increased twofold in TAT1-depleted cells compared with control cells (Fig. 2D). The frequency of microtubule breakage events that were not preceded by buckling (shown in fig. S9C and movie S10) showed no significant difference between control and TAT1-depleted cells (fig. S9D). These findings suggest that tubulin acetylation protects microtubules from breakage resulting from compressive forces.

The two known types of forces responsible for buckling and breakage of cytoplasmic microtubules are microtubule motors pushing onto anchored microtubules (*11*) and actomyosin contractility transmitted through actin-microtubule linker proteins (*19*). Contractility is likely to represent the major factor responsible for microtubule compression in nocodazole-treated cells because microtubule depolymerization leads to activation of Rho and Rho-associated kinase (ROCK), thereby increasing myosin activity and stress fiber assembly (*22*). To test the hypothesis that long-lived microtubules in TAT1-depleted cells break under actomyosin-mediated compression, we treated cells with the ROCK inhibitor Y27632 or the myosin inhibitor blebbistatin and then removed dynamic microtubules using nocodazole (Fig. 3A, and figs. S10 and S11). Pharmacological release of tension increased the mean length of nocodazole-resistant microtubules 1.5-fold in control cells (Fig. 3B). The effect of Y27632 on TAT1-depleted cells was much more dramatic, with the mean length of nocodazole-resistant microtubules increasing fourfold (Fig. 3B) and the length distribution of nocodazole-resistant microtubules approaching that of control cells in the absence of Y27632 (Fig. 3B). A statistical test for the rescue of microtubule length in TAT1-depleted cells was highly significant with Y27632 (Fig. 3B) and significant with blebbistatin (fig. S11). ROCK inhibition did not restore tubulin acetylation in TAT1-depleted cells (fig. S10, B and C). Thus, inhibition of the major Rho effectors largely restores the nocodazole-resistant microtubules lost from TAT1-depleted cells.

Because ROCK inhibition may stabilize microtubules in TAT1-depleted cells through other mechanisms than the release of compressive forces [e.g., inhibitory phosphorylation of MAPs (*23*)], we sought to release the compressive forces exerted onto microtubules in a more direct and specific manner. When cells are plated onto soft substrates made of fibronectin-coated polyacrylamide (*24*, *25*) (Fig. 3C and fig. S12), the force-dependent maturation of focal adhesions is stunted, stress fiber assembly is limited, and contractility is low (*25*). Plating cells on polyacrylamide largely rescued the length of nocodazole-resistant microtubules

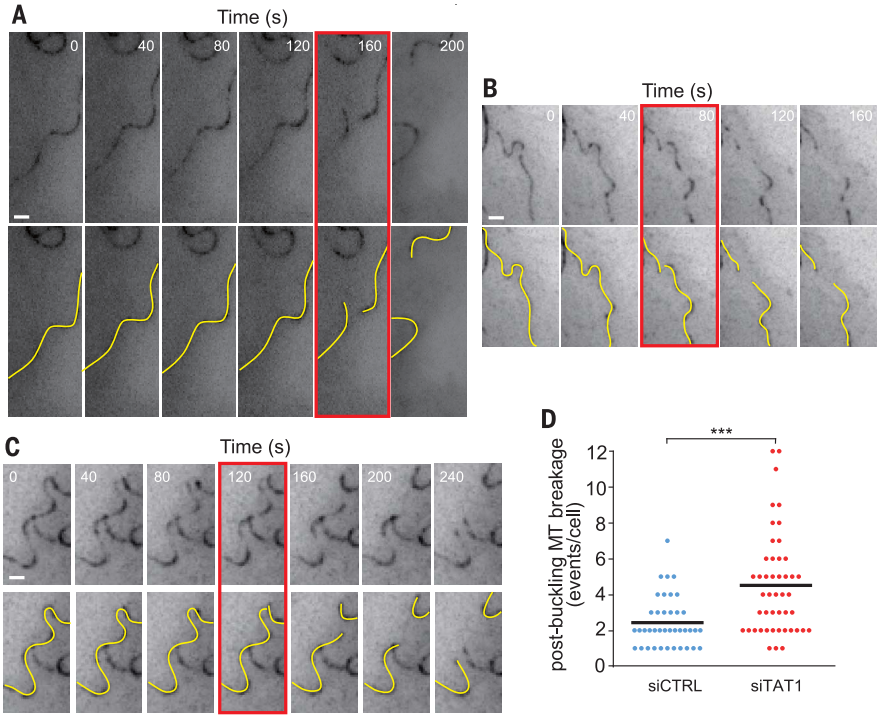

Fig. 2. TAT1 depletion sensitizes nocodazole-resistant microtubules to mechanical breakage. (**A** to **C**) Microtubules were imaged in real-time in siRNA-treated RPE-[EMTB-GFP^3] cells after at least 15 min in the presence of 2 μM nocodazole. Projection images were generated to capture microtubules across the entire cell thickness and to avoid missing microtubule segments because they left the focal plane. The yellow lines highlight microtubule behavior, and the red box indicates the first frame where rupture is clearly detected. Scale bar, 1 μm. The time series are extracted from movies S5 and fig. S7. (**D**) Microtubule breakage events preceded by buckling were counted in control and TAT1-depleted RPE-[EMTB-GFP^3] cells during the 15- to 80-min period of nocodazole treatment. N = 46 (siControl) and 52 (siTAT1) cells, six independent experiments. The bar marks the mean. Asterisks indicate t test significance values; ***$P < 10^{-4}$.

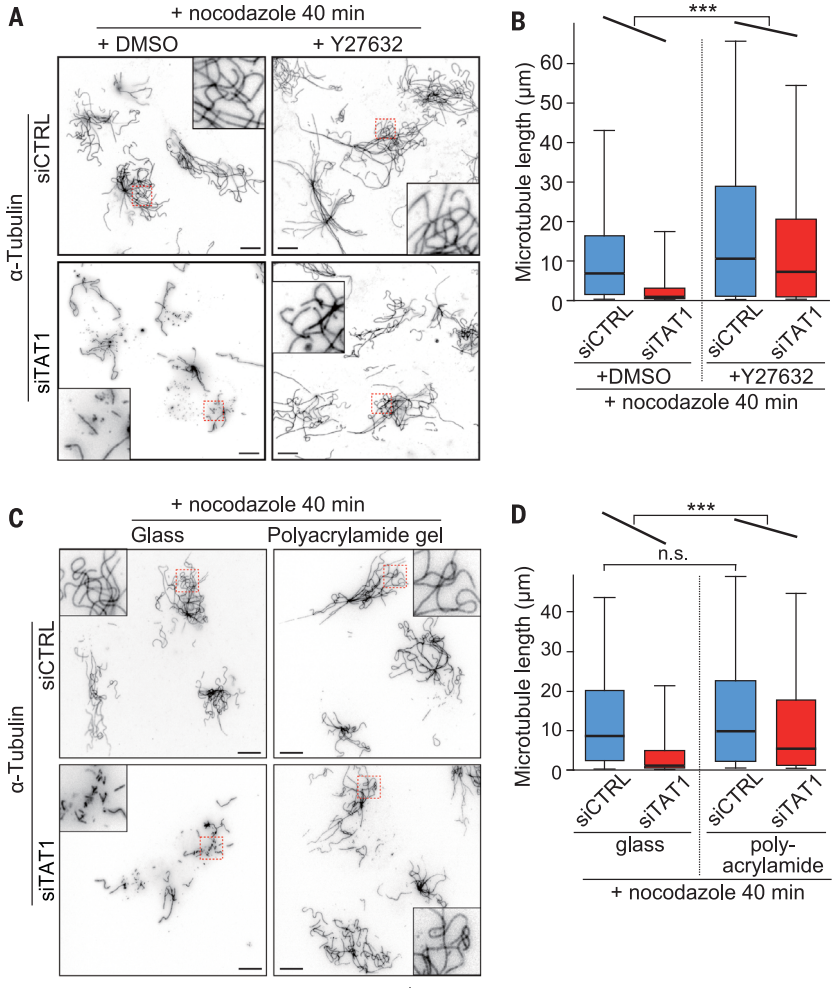

Fig. 3. Release of cell tension restores the length of nocodazole-resistant microtubules in TAT1-depleted cells. (**A**) Control and TAT1-depleted cells were treated with Y27632 or vehicle for 1 hour, then nocodazole was added for 40 min, and cells were fixed and stained for α-tubulin. (Insets) The detailed morphology of nocodazole-resistant microtubules. Scale bar, 10 μm. Insets are 10 by 10 μm. Cells before nocodazole treatment are shown in fig. S10B. Although nocodazole-resistant microtubules are few and short in the absence of TAT1, the addition of Y27632 leads to the presence of numerous long nocodazole-resistant microtubules in TAT1-depleted cells. (**B**) Measurement of individual microtubule length. The box plots follow the same conventions as Fig. 1E. N = 128 cells (2371 microtubules) siControl stained with dimethyl sulfoxide (DMSO), 369 cells (2879 microtubules) siTAT1 with DMSO, 152 cells (2462 microtubules) siControl/Y27632 and 359 cells (2446 microtubules) siTAT1/Y27632, three independent experiments. Asterisks indicate multiple regression test significance values. ***$P < 10^{-4}$. (**C**) Control and TAT1-depleted cells plated on glass coverslips (elastic modulus 50 GPa) or polyacrymide gel (PA)–coated coverslips (elastic modulus 7 kPa) were treated with nocodazole for 40 min, fixed with paraformaldehyde and stained for α-tubulin. (Insets) The detailed morphology of nocodazole-resistant microtubules. Scale bar, 10 μm (main panels). Insets are 10 by 10 μm. Cells before nocodazole treatment are shown in fig. S12. Nocodazole-resistant microtubules in TAT1-depleted cells are nearly absent when cells are plated onto glass but largely intact when cells are plated onto soft substrates. (**D**) Measurement of individual microtubule length. The box plots follow the same conventions as Fig. 1E. N = 1489 microtubules (siControl/glass), 2201 (siTAT1/glass), 1739 (siControl/PA), and 2138 (siTAT1/PA), three independent experiments. Asterisks indicate multiple regression test significance values. ***$P < 10^{-4}$. n.s. indicates Mann-Whitney U test significance value $P > 0.01$.

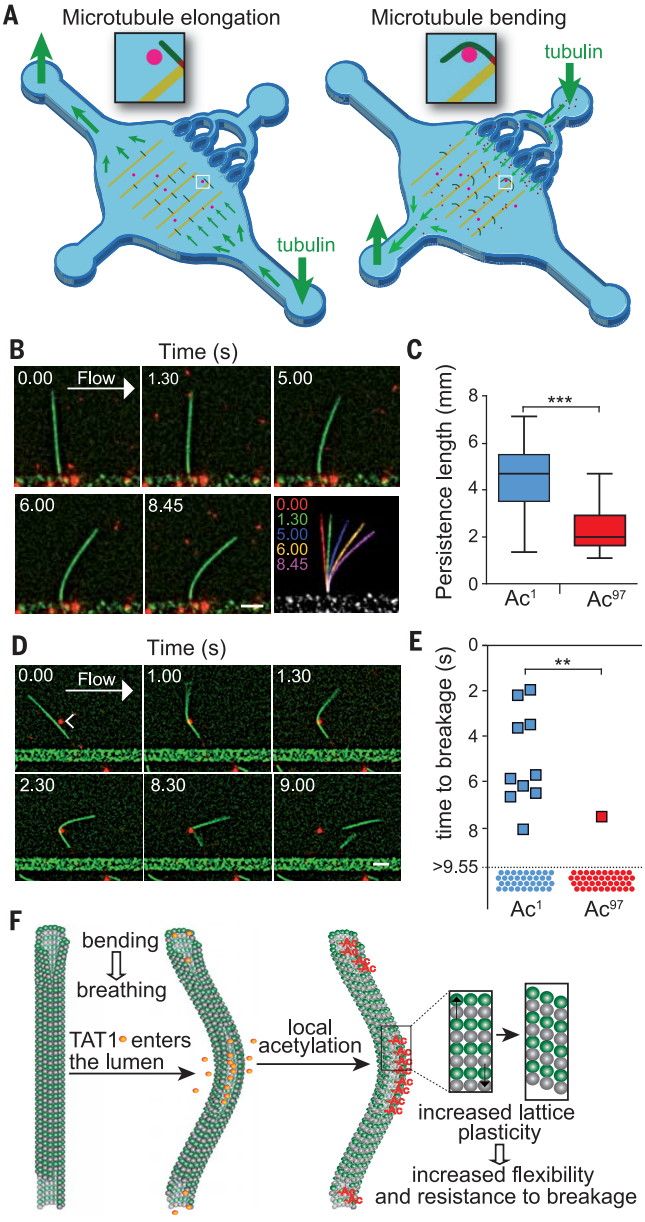

Fig. 4. Acetylation protects microtubules from mechanical breakage. (**A**) The microfluidic device used to reconstitute microtubule bending and breaking comprised two inlets and two outlets to control fluid flow along two orthogonal axes. By flowing them along the long axis, microtubule seeds (red) were grafted normally to the micropatterned lines, which forced microtubules to elongate parallel to the long axis. For the breakage assay, large beads (pink) that nonspecifically adhere to the surface were included to serve as fixed obstacles. A controlled fluid flow was applied along the short axis to subject microtubules to a normal bending force (right). The solution applied during the bending step contained free tubulin to keep microtubules dynamic and small beads (red) were added to the flowed solution to measure the flow in situ. (**B**) Time series showing the progressive bending of a microtubule (green) upon application of fluid flow. Scale bar, 5 μm. The pseudocolored image shows the overlay of successive time points. (**C**) Quantification of the persistence length of microtubules made from enzymatically acetylated and deacetylated tubulin. The box plot follows the conventions of Fig. 1G. The levels of αK40 acetylation were 97.2% (Ac^{97}) or 0.8% (Ac^{1}). N = 29 (Ac^{1}) and 25 (Ac^{97}) microtubules, three independent experiments. Asterisks indicate Mann-Whitney U test significance values, $^{***}P < 10^{-4}$. (**D**) Time series showing the breaking of a microtubule (green) upon application of fluid flow. Large beads nonspecifically adhering to the surface (arrowhead) were used as fixed obstacles to enhance microtubule bending upon flow thus resulting in microtubule rupture at the site of maximal bending. Scale bar, 10 μm. (**E**) Time taken for microtubules to break after application of flow. The shortest experimental application of flow was 9.55 s, and all microtubules not broken at 9.55 s are displayed as dots. N = 46 (Ac^{1}) and 42 (Ac^{97}) microtubules, two independent experiments. The frequency of breakage is 28% for Ac^{1} microtubules and 2% for Ac^{97} microtubules. A Mann-Whitney U test was conducted on the entire data set and asterisks indicate significance values. $^{**}P < 0.005$. (**F**) Model for regulation of microtubules mechanics by TAT1-mediated acetylation. We propose a two-step adaptive model for the mechanical stabilization of microtubules where bending results in sidewall breathing and allows TAT1 to enter the lumen. Subsequent acetylation locally modifies the mechanical properties of the microtubule to protect it against flexural breakage.

in TAT1-depleted cells (Fig. 3D). Meanwhile, the length of nocodazole-resistant microtubules was not significantly changed by plating control cells on polyacrylamide gel, and this indicates that adhesion signaling does not affect long-lived microtubules under these experimental conditions (Fig. 3D and fig. S12D). Together, the partial rescue of microtubule length by pharmacological and physical treatments strongly suggests that acetylation protects long-lived microtubules from breakage resulting from the compressive forces generated by the actomyosin cytoskeleton and makes it unlikely that acetylation prevents nocodazole-induced depolymerization. The observation that microtubule length is not fully rescued is consistent with residual forces (e.g., microtubule motors) applying stress on microtubules after these treatments.

Considering that most tissues have the stiffness of polyacrylamide gels, the observation that nocodazole-resistant microtubules are largely immune to TAT1 depletion when cells are plated on polyacrylamide gels provides a cogent explanation for the very mild phenotypes of *Tat1*$^{-/-}$ mice. The marked effects of TAT1 depletion when cells are plated on glass suggest that TAT1 will be required in specialized cell types where the stiffness is considerably higher than a few kilopascals (e.g., bone) or where microtubules are subjected to repeated mechanical stresses. Congruent with the latter hypothesis, microtubules appear damaged in touch receptor neurons of nematodes that lack TAT-1 (*16*, *26*) and tubulin acetylation sets the optimal cell stiffness for touch sensation in mammalian mechanosensory neurons (*27*). Further work examining microtubule breakage in these specialized settings is needed to establish the role of tubulin acetylation in physiological contexts.

Because some MAPs can change the mechanical properties of microtubules (*28*, *29*), acetylation could confer mechanical resistance to microtubules by altering the recruitment of specific MAPs. Alternatively, acetylation may change interactions within the lattice to directly alter microtubule mechanics (*4*). To determine whether acetylation directly protects microtubules from physical rupture, we generated pure preparations of enzymatically acetylated and deacetylated microtubules (*4*) and reconstituted microtubule breakage in vitro using a modification of our microfluidics- and micropatterning-based microtubule-bending system (*14*) (Fig. 4A). First, we confirmed that flexural rigidity is decreased by acetylation (Fig. 4, B and C) (*4*). By including large stationary beads in the path of the bending microtubules, the microtubule sharply kinked and frequently broke at the site of maximal curvature (Fig. 4D). Although nearly one-third of the deacetylated microtubules (Ac^{1}) ruptured under the mechanical stress, only 2% of the highly acetylated microtubules (Ac^{97}) broke under the same conditions (Fig. 4E). Thus, acetylation directly protects microtubules from rupture. We propose that, by weakening interprotofilament interactions (*4*), acetylation increases lattice plasticity and limits the spread of preexisting lattice damage under repeated mechanical stress and thus protects microtubules from material fatigue (*4*) or mechanical breakage (Fig. 4E). Because acetylation is enriched in regions of high curvature (Fig. 1G), microtubule mechanics are likely to be modified locally. Furthermore, cyclic stretch of cells increases acetylation (*30*), and lattice openings are found in bent segments of microtubules (*31*). Stress-induced bending may thus produce transient openings that let TAT1

access the microtubule lumen in areas experiencing the highest stress (*32*) and result in an adaptive and local increase in mechanical resilience (Fig. 4F).

REFERENCES AND NOTES

1. R. Li, G. G. Gundersen, *Nat. Rev. Mol. Cell Biol.* **9**, 860–873 (2008).
2. Y. Song, S. T. Brady, *Trends Cell Biol.* **25**, 125–136 (2015).
3. C. Janke, J. C. Bulinski, *Nat. Rev. Mol. Cell Biol.* **12**, 773–786 (2011).
4. D. Portran, L. Schaedel, Z. Xu, M. Théry, M. V. Nachury, *Nat. Cell Biol.* **19**, 391–398 (2017).
5. A. D.-A. Tran *et al.*, *J. Cell Sci.* **120**, 1469–1479 (2007).
6. I. Topalidou *et al.*, *Curr. Biol.* **22**, 1057–1065 (2012).
7. N. Kalebic *et al.*, *Mol. Cell. Biol.* **33**, 1114–1123 (2013).
8. B. Neumann, M. A. Hilliard, *Cell Rep.* **6**, 93–103 (2014).
9. M. L. Valenstein, A. Roll-Mecak, *Cell* **164**, 911–921 (2016).
10. C. P. Brangwynne *et al.*, *J. Cell Biol.* **173**, 733–741 (2006).
11. A. D. Bicek *et al.*, *Mol. Biol. Cell* **20**, 2943–2953 (2009).
12. P. Robison *et al.*, *Science* **352**, aaf0659 (2016).
13. T. Hawkins, M. Mirigian, M. S. Yasar, J. L. Ross, *J. Biomech.* **43**, 23–30 (2010).
14. L. Schaedel *et al.*, *Nat. Mater.* **14**, 1156–1163 (2015).
15. C. Aumeier *et al.*, *Nat. Cell Biol.* **18**, 1054–1064 (2016).
16. J. G. Cueva, J. Hsin, K. C. Huang, M. B. Goodman, *Curr. Biol.* **22**, 1066–1074 (2012).
17. G. Geuens *et al.*, *J. Cell Biol.* **103**, 1883–1893 (1986).
18. D. J. Odde, L. Ma, A. H. Briggs, A. DeMarco, M. W. Kirschner, *J. Cell Sci.* **112**, 3283–3288 (1999).
19. S. L. Gupton, W. C. Salmon, C. M. Waterman-Storer, *Curr. Biol.* **12**, 1891–1899 (2002).
20. E. J. Ezratty, M. A. Partridge, G. G. Gundersen, *Nat. Cell Biol.* **7**, 581–590 (2005).
21. K. Faire *et al.*, *J. Cell Sci.* **112**, 4243–4255 (1999).
22. Y.-C. Chang, P. Nalbant, J. Birkenfeld, Z.-F. Chang, G. M. Bokoch, *Mol. Biol. Cell* **19**, 2147–2153 (2008).
23. M. Amano, M. Nakayama, K. Kaibuchi, *Cytoskeleton* **67**, 545–554 (2010).
24. R. J. Pelham Jr., Y. Wang, *Proc. Natl. Acad. Sci. U.S.A.* **94**, 13661–13665 (1997).
25. J. Solon, I. Levental, K. Sengupta, P. C. Georges, P. A. Janmey, *Biophys. J.* **93**, 4453–4461 (2007).
26. I. Topalidou, M. Chalfie, *Proc. Natl. Acad. Sci. U.S.A.* **108**, 19258–19263 (2011).
27. S. J. Morley *et al.*, *eLife* **5**, 618 (2016).
28. H. Felgner *et al.*, *J. Cell Biol.* **138**, 1067–1075 (1997).
29. D. Portran *et al.*, *Mol. Biol. Cell* **24**, 1964–1973 (2013).
30. D. A. Hoey, M. E. Downs, C. R. Jacobs, *J. Biomech.* **45**, 17–26 (2012).
31. I. A. T. Schaap, C. Carrasco, P. J. de Pablo, F. C. MacKintosh, C. F. Schmidt, *Biophys. J.* **91**, 1521–1531 (2006).
32. C. Coombes *et al.*, *Proc. Natl. Acad. Sci. U.S.A.* **113**, E7176–E7184 (2016).

ACKNOWLEDGMENTS

We are grateful to Z. Werb for hosting experiments in her laboratory, S. Triclin and L. Kurzawa for investigating microtubule lifetime in TAT1-depleted cells, D. Nager and F. Ye for assistance with statistical analysis, T. Vignaud and Q. Tseng for preparing polyacrylamide-coated coverslips, to G. G. Gundersen for the detyrosinated tubulin antibody, to C. Bulinski for p3xGFP-EMTB, to C. Janke for the spastin cDNA, and to F. McNally for the katanin p60 construct. This work was funded by Stanford School of Medicine (Deans' Fellowships to Z.X. and A.A.); U.S. Department of Defense (BC103963, Z.X.); National Cancer Institute, NIH (CA108462, Z.X., and CA057621, Z. Werb); NIH funding (GM089933) to M.V.N.; the Human Frontier Science Program (RGY0088, M.V.N. and M.T.); the French National Research Agency (ANR) (14-CE09-0014-02, M.T.); and the Palo Alto Veterans Administration (M.P.M.). M.V.N., M.T., and Z.X. conceived and coordinated the project with help from M.P.M; M.V.N. and Z.X. wrote the paper with contributions from all authors; L.S., M.T., and J.G. developed the microfluidics system and performed the bending and breakage experiments; D.P. prepared tubulin with defined acetylation level; A.A. conducted experiments with MEFs, and Z.X. conducted all other experiments. Data described can be found in the main figures and supplementary materials. The authors declare no conflict of interest.

SUPPLEMENTARY MATERIALS

www.sciencemag.org/content/356/6335/328/suppl/DC1
Materials and Methods
Supplementary Text
Figs. S1 to S12
References (*33*–*50*)
Movies S1 to S13

25 August 2016; accepted 24 March 2017
10.1126/science.aai8764

Acetylation keeps microtubules strong

Cells need microtubules for intracellular transport and to avoid being crushed. On investigating microtubule breakage in live fibroblasts, Xu *et al.* found that if they were not acetylated, long-lived microtubules underwent frequent rupture after buckling. Acetylation makes microtubules more mechanically stable, facilitates sliding between filaments, and makes the lattice more plastic.

Science, this issue p. 328